

Helicity exchange and symmetry breaking of in-plane phonon scattering of h-BN probed by polarized Raman spectroscopy

Cite as: Appl. Phys. Lett. **121**, 182203 (2022); <https://doi.org/10.1063/5.0114075>

Submitted: 25 July 2022 • Accepted: 17 October 2022 • Published Online: 01 November 2022

 Shih-Po Chien,  Yu-Chen Chang,  Kristan Bryan Simbulan, et al.



View Online



Export Citation



CrossMark



Trailblazers. 

Meet the Lock-in Amplifiers that measure microwaves.

 Zurich Instruments [Find out more](#)

Helicity exchange and symmetry breaking of in-plane phonon scattering of h-BN probed by polarized Raman spectroscopy

Cite as: Appl. Phys. Lett. **121**, 182203 (2022); doi: [10.1063/5.0114075](https://doi.org/10.1063/5.0114075)

Submitted: 25 July 2022 · Accepted: 17 October 2022 ·

Published Online: 1 November 2022



View Online



Export Citation



CrossMark

Shih-Po Chien,¹ Yu-Chen Chang,¹ Kristan Bryan Simbulan,² Shantanu Saha,^{3,a)} Yu-Fan Chiang,¹ Rajendra K. Saroj,⁴ Cyu-Chul Yi,^{4,5} Shamsul Arafin,^{3,b)} Ting-Hua Lu,^{1,b)} and Yann-Wen Lan^{1,b)}

AFFILIATIONS

¹Department of Physics, National Taiwan Normal University, Taipei 116, Taiwan

²Department of Mathematics and Physics, University of Santo Tomas, Manila, Philippines

³Department of Electrical and Computer Engineering, The Ohio State University, Columbus, Ohio 43210, USA

⁴Department of Physics and Astronomy, Institute of Applied Physics, Seoul National University, Seoul 151-747, Republic of Korea

⁵Research Center for Novel Epitaxial Quantum Architectures, Seoul National University, 1, Gwanak-ro, Gwanak-gu, Seoul 08826, South Korea

^{a)}Present address: Department of Electrical, Electronics and Communication Engineering, GITAM School of Technology, GITAM (Deemed to be University), Hyderabad 502329, Telangana, India.

^{b)}Authors to whom correspondence should be addressed: arafin.1@osu.edu; thlu@ntnu.edu.tw; and ywlan@ntnu.edu.tw

ABSTRACT

Due to its atomic thickness and insulating nature, hexagonal boron nitride (h-BN) is considered to be one of the most promising substrates and gate insulating materials for two-dimensional electronic devices. In this study, polarized Raman spectroscopy was employed to uncover the effects of polarized incident light on the optical properties of h-BN phonon modes. Our measured polarization-resolved Raman spectra indicate that the symmetrical nature and the broken symmetry of degenerate phonon modes from h-BN are induced by linearly and elliptically polarized light, respectively. Moreover, a helicity exchange was observed between the excitation of circularly polarized light and the resulting opposite circular polarization of scattered light from h-BN. The measured phenomena were modeled on the basis of Raman tensors and Jones calculus to eventually calculate the amplitude coefficients of two orthogonal in-plane phonon modes. Hence, our experimental study provides a holistic understanding of the vibrational modes in h-BN, which is expected to enhance the knowledge of physical mechanisms such as heat capacity and thermal and electrical conductivities of this layered material.

Published under an exclusive license by AIP Publishing. <https://doi.org/10.1063/5.0114075>

Boron nitride (BN) forms various polymorphs with distinct physical characteristics. Strong hardness, high thermal conductivity, and chemical stability have made BN a favorable material utilized as a protective coating and abrasive tool for many years.¹ BN is characterized by several physical properties associated with carbon polymorphs due to its analogous structures.² h-BN is a dangling-bond-free layered material providing an ultra-smooth surface, which is beneficial to form a van der Waals (vdW) heterostructure with graphene, transition metal dichalcogenides (TMDCs), and many other two-dimensional (2D) materials.² Possessing an insulating nature, h-BN has been widely applied in many electronic devices as a dielectric layer.³ Moreover, h-BN is also considered to be an adequate supporting substrate in

graphene-based devices, as the atomic arrangement of h-BN corresponds to that of graphene.^{4,5} Recently, some researchers have started to focus on applications requiring wide-bandgap characteristics, which has made h-BN a promising material to construct optical emission and detection devices for ultraviolet (UV) light.^{2,6}

Raman spectroscopy is a nondestructive method to investigate the vibrational modes of materials.^{7,8} This technology has been widely used to characterize material properties such as thickness and stacking order of 2D materials or vdW heterostructures and to further identify their molecular composition.^{9,10} The Raman peak of the in-plane vibrational mode (E_{2g}) in single crystal h-BN has been found to be at $\sim 1366 \text{ cm}^{-1}$.¹¹⁻¹⁴ The peak position shows slight blueshifts

($\sim 4 \text{ cm}^{-1}$) as the number of layers increases up to the first few layers,^{11,12} some random shifts induced by strain have also been reported by Gorbachev *et al.*, which are negligible in multilayer h-BN.¹¹ Beside from its peak position, the Raman intensity of the E_{2g} mode in h-BN can also be used to identify the thickness of the material.

A derivative technology called polarized Raman spectroscopy employing polarized incident light can be used to probe the polarization of scattered light, which involves information such as the orientation of molecules and the symmetry of vibrational modes.^{15,16} Previously, Huang *et al.* added optical components to convert incident light into elliptically polarized light, which possesses an extra degree of freedom for polarization.¹⁷ In response, the degenerate in-plane E_{2g} mode in MoS₂ was found to have a symmetry-breaking behavior, in which the amplitudes of the vibrations along the x and y directions were distinct. Additionally, Chen *et al.* demonstrated the use of a polarized Raman system to investigate the helicities of Raman signals from several kinds of TMDCs induced by circularly polarized incident light.¹⁸

This work is focused on investigating the relationship between incident light having various polarizations and the vibrational mode of h-BN using polarized Raman spectroscopy. The polarization of incident light was controlled by a quarter-wave plate (QWP) and a half-wave plate (HWP) before hitting the sample. The resulting Raman signal from the sample was then detected and resolved through the analyzer, leading to the identification of its polarization or helicity. Consequently, the measured signals indicate the symmetrical nature and the broken symmetry of phonon modes induced by linearly and elliptically polarized light, respectively. This phenomenon was modeled by fitting the amplitudes of the vibrational modes from Raman tensors and Jones calculus. Meanwhile, a helicity exchange was also evident in the observation of the opposite circularly polarized scattered light resulting from the excitation light. This study uncovers results from the interaction of incident light possessing different polarization states and h-BN, demonstrating the extraordinary optical properties of the induced Raman scattered light. Hence, the findings of this work are envisioned to build a further understanding of the vibrational modes of h-BN.

To provide insight into the response of the phonon modes of h-BN to an incident polarized light, polarization-resolved Raman spectra of multilayer h-BN on both sapphire and SiO₂/Si substrates were recorded and analyzed in this work. Incident linearly and elliptically polarized beams were employed for polarization-resolved spectral analyses, while left-handed and right-handed circularly polarized light was used for helicity-resolved spectral studies. The polarization state of the incident light, $|E_i\rangle$, can be described by the expression¹⁷

$$|E_i\rangle = \begin{pmatrix} E_x \\ e^{i\phi} E_y \end{pmatrix}, \quad (1)$$

where E_x and E_y are the mutually orthogonal electric field components of E_i and ϕ is the phase difference between these two components. The amplitudes and phase determine the light's polarization state. For instance, a vertical linearly polarized light can be characterized by $E_x = 0$, $E_y = 1$, and $\phi = 0$; a circularly polarized light by $E_x = E_y = 1$, and $\phi = \pm \frac{\pi}{2}$; and an elliptically polarized light by $E_x \neq E_y$ or ϕ between 0 and $\pm \frac{\pi}{2}$. Mathematically, the relationship between the electric field vector of the incident light and that of the Raman scattered

light E_s , corresponding to a phonon mode ν , is characterized through the Raman tensor $R(\nu)$ of the material.¹⁷ The dominant phonon mode of h-BN is the degenerate in-plane E_{2g} , which can be decomposed into two components: one along the x -direction E_{2gx} and the other along the y -direction E_{2gy} with their corresponding Raman tensors defined as $R(E_{2gx}) = \begin{pmatrix} d & 0 \\ 0 & -d \end{pmatrix}$ and $R(E_{2gy}) = \begin{pmatrix} 0 & d \\ d & 0 \end{pmatrix}$. By noting the unit vector of the scattered light

$$\langle |E_s(\theta)\rangle = (\cos \theta \quad \sin \theta), \quad (2)$$

that is oriented at a polarization angle, the total Raman intensity as a function of θ can be calculated as

$$I(\theta) = \sum_{\nu} c_{\nu} \left| \langle E_s(\theta) | R(\nu) | E_i \rangle \right|^2 = m \times I_{E_{2gx}}(\theta) + n \times I_{E_{2gy}}(\theta), \quad (3)$$

where $I_{E_{2gx}}$ and $I_{E_{2gy}}$ are the Raman intensities of the two orthogonal phonon modes. The amplitude coefficients c_{ν} for both E_{2gx} and E_{2gy} modes are specifically expressed as m and n , respectively. The values of the coefficients are determined in this work by fitting experimental data with Eq. (3).

Multilayered bulk-like h-BN thin films used in the study were grown by chemical vapor deposition (CVD). A detailed growth procedure of the h-BN films can be found in a previous report.¹⁹ Two kinds of samples with different substrates were used for measurements. Sample 1 is a multilayer (94 ML) h-BN film grown on a sapphire substrate by CVD. Later on, the film was transferred onto a SiO₂/Si substrate to yield sample 2. Atomic force microscopy (AFM) images of the two samples exhibit h-BN thicknesses of $\sim 443 \text{ nm}$ [Fig. 1(c)] and $\sim 18 \text{ nm}$ [Fig. 1(d)] for samples 1 and 2, respectively. The bulk-like thickness prevents substrate dependency that has been observed in the Raman spectrum of graphene due to film-substrate coupling.²⁰ Raman spectra of each of the samples [Figs. 1(e) and 1(f)] were taken to further identify the presence of h-BN layers on the substrates, yielding an expected Raman peak position of the E_{2g} mode centered at $\sim 1370 \text{ cm}^{-1}$.^{21,22} The Raman peak at 1453 cm^{-1} in Fig. 1(f) refers to the third order transverse optical mode (3TO) of SiO₂.²³

The experimental setup consists of a micro-Raman spectrometer with additional optical elements to conduct polarization-resolved measurements. A polarizer was inserted between the measured samples and the spectrometer to analyze the Raman spectra from scattered light at a specific polarization angle θ . The polarizer is then known herein as the analyzer, in which θ was adjusted from 0° to 360° in 15° increments. A 532 nm linearly polarized solid-state laser was used to excite the measured samples through a $50 \times$ (NA = 0.75) objective lens. The orientation of this incident light is controlled by the HWP as shown in Fig. 2(a), giving it either a horizontal or vertical polarization state.

The Raman measurements were recorded from sample 1, and the corresponding polarized intensities were plotted using horizontally and vertically polarized incident light as shown in Figs. 2(b) and 2(c), respectively. In these conditions, the polar plots show that the h-BN's E_{2g} has an isotropic polarization property, i.e., the Raman intensity is uniform in various orientation angles, implying that the x and y components of E_{2g} are triggered fairly. A close reason why a not-so-symmetrical polar plot was observed is the small movement of the sample stage due to long exposure time for the weak Raman signal. A more symmetrical polar plot has been recorded and shown in Fig. S1.

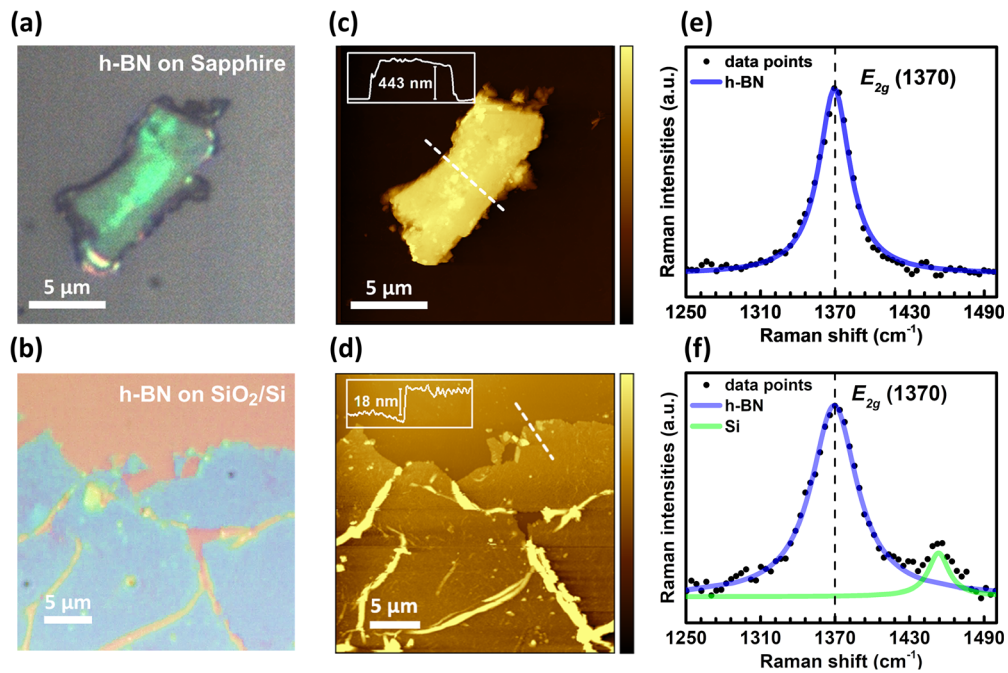


FIG. 1. Characterization of h-BN samples. Optical images of multilayer h-BN on (a) a sapphire substrate (sample 1) and (b) on a SiO₂/Si substrate (sample 2). AFM images of (c) sample-1 and (d) sample-2 with insets showing AFM profiles taken along the dashed lines indicated in their respective optical images. Raman spectra of a multilayer h-BN E_{2g} mode for (e) sample 1 and (f) sample 2.

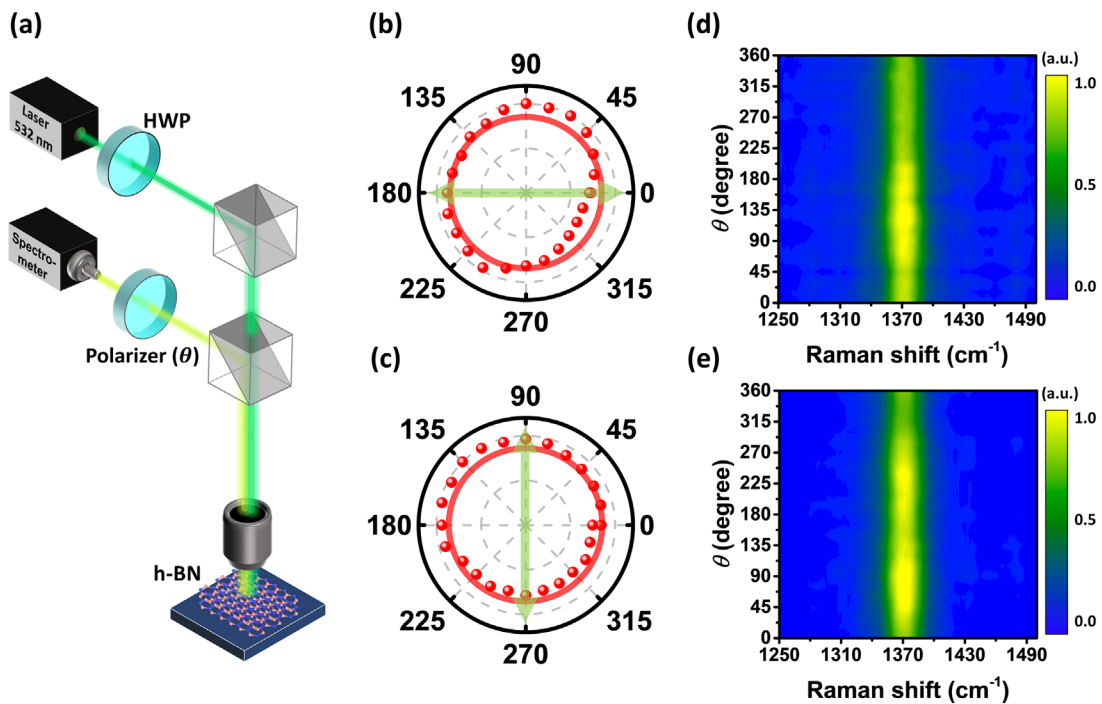


FIG. 2. h-BN on sapphire (sample 1) excited by linearly polarized light. (a) The schematic diagram of the polarization-resolved Raman spectroscopy setup employing linearly polarized excitation light. The green line illustrates the incident light, while the yellow line is for the scattered light. The normalized polar plots of scattered light intensities excited by the (b) horizontal and (c) vertical polarization light, where the green arrows imply the polarization of the incident laser. The solid red circles are fitting curves of the E_{2g} mode showing isotropic intensities in all directions. (d) and (e) Color map of Raman intensities as a function of the detection angle θ .

TABLE I. The fitted parameters of Raman intensities induced by linearly polarized excitation light.

	Horizontal linear polarization	Vertical linear polarization
Incident light	$E_x = 1, E_y = 0, \phi = 0$	$E_x = 0, E_y = 1, \phi = 0$
E_{2g}	$I(E_{2gx}) = m(d \cos \theta)^2$ $I(E_{2gy}) = n(d \sin \theta)^2$ ($m = n = 1/\sqrt{2}, d = 1$)	$I(E_{2gx}) = m(-d \sin \theta)^2$ $I(E_{2gy}) = n(d \cos \theta)^2$ ($m = n = 1/\sqrt{2}, d = 1$)

Meanwhile, the color maps of the Raman measurements induced by horizontally [Fig. 2(d)] and vertically [Fig. 2(e)] polarized excitation light further show that both have almost steady Raman peak positions, all equivalent to $\sim 1370 \text{ cm}^{-1}$. To further analyze the compositions of the E_{2g} mode, data points in each polar plot were fitted by the Raman intensity function in Eq. (3), and the values for the amplitude coefficients m and n were acquired. The normalized parameters of the incident light and the fitted values of the amplitude coefficients of the respective Raman intensities are listed in Table I. In these analyses, the isotropic properties of the polarized Raman intensities in Figs. 2(b) and 2(c) reflect the equivalence of the m and n values. Similar measurements and fitting parameters were taken from sample 2, which are presented in Fig. S2 and Table SI, respectively.

The incident light was then transmitted with specific helicities to observe the helicity-resolved Raman spectra of the samples. The spectroscopy setup was assembled with a QWP in front of the objective lens, as shown in Fig. 3(a), to convert the incident light's polarization

from linear to circular. A right-handed (left-handed) helicity is produced when an incident linearly polarized light passes through the QWP at an angle of 45° (-45°) with respect to the QWP's fast axis. Since the incident and scattered light share the same optical path, the determination of helicity can be resolved by the use of the QWP and polarizer combination with comparing the scattered light to the incident light. Hence, the detected polarization of the scattered light in the spectrometer is linear, and its orientation indicates the scattered light's helicity right after leaving the sample. Figures 3(b) and 3(c) show the detected E_{2g} intensity polar graphs of the scattered light from sample 2, including that of the incident light. Apparently, the orientation of the scattered light's helicity-resolved polarization is perpendicular to that of the incident light, implying that these two have opposite helicities, i.e., a helicity exchange occurred between the incident light approaching the sample and the resulting scattered light from the sample. The details of the helicity-resolved Raman spectra are presented in Figs. 3(d) and 3(e). In the case of right-handed circularly polarized excitation light, Fig. 3(d) depicts the maximum intensity with left-handed helicity labeled as RL and the minimum intensity with right-handed helicity labeled as RR. The similar Raman spectra for the case of left-handed circularly polarized excitation were plotted in Fig. 3(e). Color maps of the helicity-resolved Raman intensities are shown in Figs. 3(f) and 3(g). The normalized parameters of the incident light and the fitted values for the amplitude coefficients of the respective helicity-resolved Raman intensities are listed in Table II, which accurately models the recorded experimental data. Similarly observed phenomenon and fitting parameters conducted on sample 1 are presented in Fig. S3 and Table SII, respectively.

Moving the QWP right after the HWP, as in Fig. 4(a), produces elliptically polarized incident light. A right-handed (left-handed)

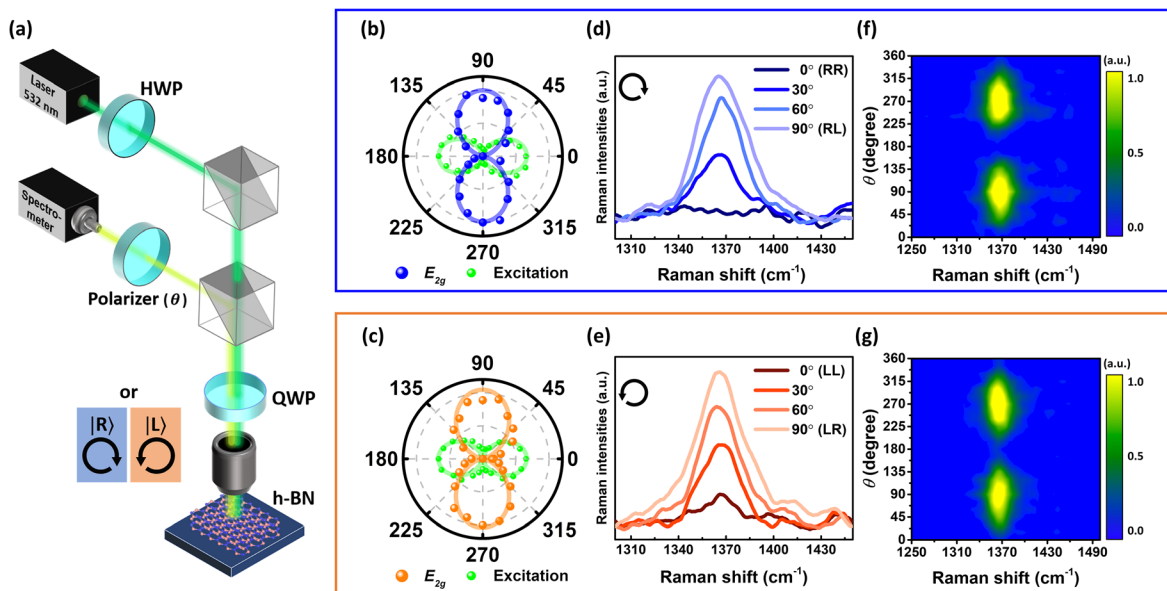


FIG. 3. h-BN on SiO_2/Si (sample 2) excited by circularly polarized light. (a) Schematic of the helicity-resolved Raman spectroscopy setup. A QWP was placed in front of the objective lens to generate purely circularly polarized excitation light. The black circle arrows indicate the helicities of the incident light. Normalized polar plots of the scattered light excited by (b) right-handed and (c) left-handed circularly polarized incident light along with their corresponding helicity-resolved Raman spectra (d) and (e), respectively. (f) and (g) Color maps of the helicity-resolved Raman intensities as a function of θ . The solid dumbbell curves having the same color as the scatter data points in (b) and (c) are the fitting results for the helicity-resolved E_{2g} (scattered) intensities, whereas the green curves indicate the numerical polarization of the incident light.

TABLE II. The fitted parameters of helicity-resolved Raman intensities.

	Right-handed circular polarization	Left-handed circular polarization
Incident light	$E_x = \frac{1}{\sqrt{2}}, E_y = \frac{1}{\sqrt{2}},$ $\phi = \frac{\pi}{2}$	$E_x = \frac{1}{\sqrt{2}}, E_y = \frac{1}{\sqrt{2}},$ $\phi = -\frac{\pi}{2}$
E_{2g}	$I(E_{2gx}) = m (d\sqrt{2} \sin \theta)^2$ $I(E_{2gy}) = n (d\sqrt{2} \sin \theta)^2$ ($m = n = 1/\sqrt{2}, d = 1$)	$I(E_{2gx}) = m (d\sqrt{2} \sin \theta)^2$ $I(E_{2gy}) = n (d\sqrt{2} \sin \theta)^2$ ($m = n = 1/\sqrt{2}, d = 1$)

elliptical polarization was generated by adjusting the combination of the QWP and HWP. Such an approach is similar to that described by Huang *et al.*¹⁷ Elliptically polarized light consists of non-uniform electric fields along x and y axes, which may induce unequal intensities of the x (E_{2gx}) and y (E_{2gy}) components of the E_{2g} phonon mode. To observe this experimentally, we perform polarization-resolved measurements to acquire polar plots [Figs. 4(b) and 4(c)] by utilizing both right- and left-handed elliptically polarized light illuminating on sample 1. The selected polarization-resolved Raman spectra for the polarizer orientated at $\theta = 45^\circ, 75^\circ, 105^\circ,$ and 135° are displayed in Figs. 4(d) and 4(e), and color maps as a function of θ are also shown in Figs. 4(f) and 4(g). Similar results were observed in sample 2 as presented in Fig. S4. By observing Figs. 4(b) and 4(c), one can see that the major axes of the elliptically polarized scattered light are perpendicular to those of their corresponding incident light. The amplitude coefficients were likewise analyzed using fitting functions derived from the

Jones calculus as shown in Table III. The results from the measured data in both right- and left-handed incident helicity cases indicated that the fitting amplitude coefficients of E_{2gx} were greater than that of E_{2gy} , reflecting the asymmetricity of the in-plane phonon mode (E_{2g}) in h-BN. One of the possible mechanisms is that the relative phase of the elliptically polarized light may induce the Fröhlich interaction by altering the macroscopic electric field,²⁴ leading to the Raman scattered light having different amplitude relative phases along E_{2gx} and E_{2gy} directions. The calculated parameters for sample 2 are also shown the same behavior in Table SIII. The detailed Raman tensor calculation for elliptically polarized light is described in Figs. S5 and S6 of the supplementary material.

In conclusion, polarization-resolved measurements of the Raman intensities for h-BN's E_{2g} mode have been demonstrated. Incident light with linear, circular, and elliptical polarization states were utilized to reveal the behavior of the E_{2g} polarization with respect to that of incident light. Linearly polarized light excited uniform in-plane vibrational Raman intensity in both x (E_{2gx}) and y (E_{2gy}) directions, whereas incident elliptically polarized light could break the symmetry of the E_{2gx} and E_{2gy} vibrations leading to asymmetric in-plane lattice vibration owing to the potential inducement of Fröhlich interaction. It was also found that when an incident circularly polarized light was illuminated on h-BN, opposite helicities between the incident light and the Raman scattering light were apparently demonstrated. These properties were observed in both multilayer h-BN on sapphire (sample 1) and SiO₂/Si (sample 2) substrates without showing substrate dependence due to the thickness of the samples already reaching the bulk limit. This work provided a method to manipulate the vibrational mode of h-BN using the polarization of incident light. By understanding the phenomena and its mechanism, this can be extended to other

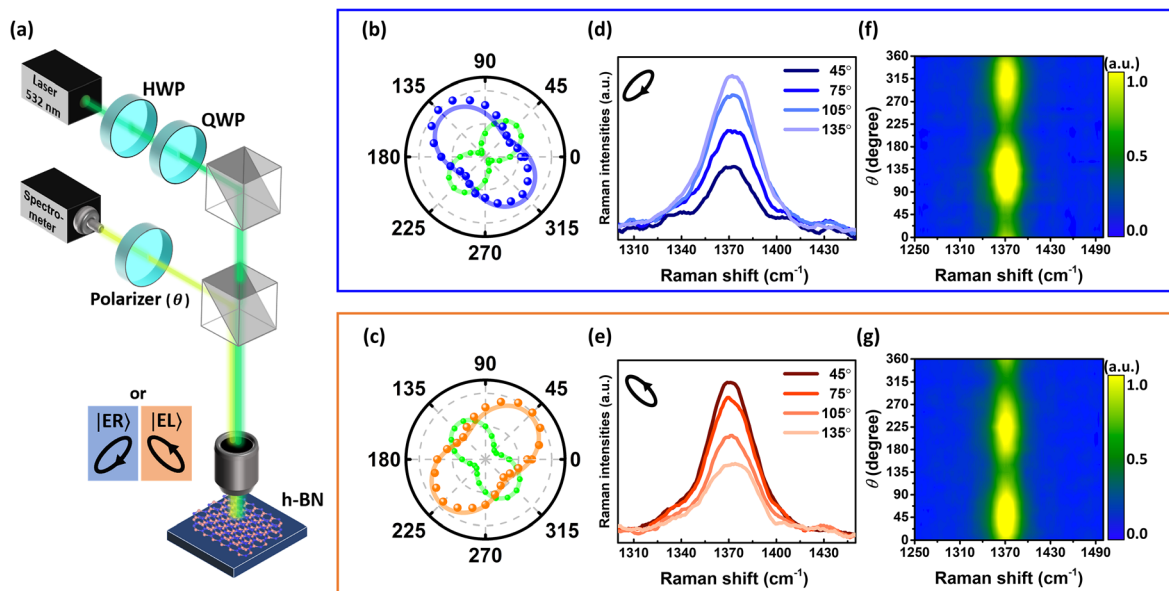


FIG. 4. h-BN on sapphire (sample 1) excited by elliptically polarized light. (a) Schematic of the polarization-resolved Raman spectroscopy setup. The elliptically polarized excitation light, denoted as $|ER\rangle$ and $|EL\rangle$, was generated through the appropriately oriented half-wave and quarter-wave plates. The black arrows show the opposite helicity orientations of the elliptically polarized light. (b) and (c) Normalized polar plots of the scattered light intensities induced by incident light $|ER\rangle$ and $|EL\rangle$, respectively. The solid curves are the fitting results for the E_{2g} mode, and the green curves show polarizations of incident light. (d) and (e) The selected polarization-resolved Raman spectra corresponding to the polar plots collected at $\theta = 45^\circ$ – 135° . (f) and (g) Color maps of Raman intensities as a function of θ .

TABLE III. The fitted parameters of Raman intensities for elliptically polarized excitation light.

	Right-handed elliptical polarization	Left-handed elliptical polarization
Incident light	$E_x = \frac{1}{\sqrt{2}}, E_y = \frac{1}{\sqrt{2}}, \phi = 0.20\pi$	$E_x = \frac{1}{\sqrt{2}}, E_y = \frac{1}{\sqrt{2}}, \phi = 0.70\pi$
E_{2g}	$I(E_{2gx}) = m((d \cos \theta - d \cos \phi \sin \theta)^2 + (d \sin \phi \sin \theta)^2)$ $I(E_{2gy}) = n((d \sin \theta + d \cos \phi \cos \theta)^2 + (d \sin \phi \cos \theta)^2)$ $(m = 0.47, n = 0.19, d = 1)$	$I(E_{2gx}) = m((d \cos \theta - d \cos \phi \sin \theta)^2 + (d \sin \phi \sin \theta)^2)$ $I(E_{2gy}) = n((d \sin \theta + d \cos \phi \cos \theta)^2 + (d \sin \phi \cos \theta)^2)$ $(m = 0.56, n = 0.14, d = 1)$

2D materials, and more possible applications in optical components and optoelectronics are expected to be developed.

See the [supplementary material](#) for the linearly, circularly, and elliptically polarized light induced polarization-resolved Raman spectra along with the calculated parameters on other h-BN samples and numerically calculated polarization of scattered light excited by elliptically polarized light.

This work was supported by the Ministry of Science and Technology, Taiwan under Contract Nos. MOST 108-2112-M-003-010-MY3, MOST 111-2119-M-008-003-MBK, and MOST 108-2112-M-003-009. This work was also supported in part by the Ministry of Education of Taiwan and the Taiwan Semiconductor Research Institute.

AUTHOR DECLARATIONS

Conflict of Interest

The authors have no conflicts to disclose.

Author Contributions

Shih-Po Chien: Data curation (lead); Formal analysis (equal); Investigation (equal); Writing – original draft (equal). **Yann-Wen Lan:** Conceptualization (equal); Supervision (equal); Validation (equal); Writing – review & editing (equal). **Yu-Chen Chang:** Data curation (equal); Formal analysis (equal); Investigation (equal); Writing – original draft (equal). **Kristan Bryan Simbulan:** Investigation (equal); Methodology (equal); Writing – original draft (equal). **Shantanu Saha:** Data curation (equal); Investigation (equal); Methodology (equal). **Yu-Fan Chiang:** Data curation (equal); Investigation (equal); Methodology (equal). **Rajendra Kumar Saroj:** Investigation (equal); Methodology (equal). **Gyu-Chul Yi:** Investigation (equal); Methodology (equal). **Shamsul Arafin:** Supervision (equal); Validation (equal); Writing – review & editing (equal). **Ting-Hua Lu:** Conceptualization (equal); Funding acquisition (equal); Supervision (equal); Writing – review & editing (equal).

DATA AVAILABILITY

The data that support the findings of this study are available from the corresponding authors upon reasonable request.

REFERENCES

- S. N. Monteiro, A. L. D. Skury, M. G. de Azevedo, and G. S. Bobrovitchii, “Cubic boron nitride competing with diamond as a superhard engineering material—An overview,” *J. Mater. Res. Technol.* **2**, 68 (2013).
- N. Izyumskaya, D. O. Demchenko, S. Das, Ü. Özgür, V. Avrutin, and H. Morkoç, “Recent development of boron nitride towards electronic applications,” *Adv. Electron. Mater.* **3**, 1600485 (2017).
- K. K. Kim, A. Hsu, X. Jia, S. M. Kim, Y. Shi, M. Dresselhaus, T. Palacios, and J. Kong, “Synthesis and characterization of hexagonal boron nitride film as a dielectric layer for graphene devices,” *ACS Nano* **6**, 8583 (2012).
- C. R. Dean, A. F. Young, I. Meric, C. Lee, L. Wang, S. Sorgenfrei, K. Watanabe, T. Taniguchi, P. Kim, and K. Shepard, “Boron nitride substrates for high-quality graphene electronics,” *Nat. Nanotechnol.* **5**, 722 (2010).
- A. Nag, K. Raidongia, K. P. S. Hembam, R. Datta, U. V. Waghmare, and C. N. R. Rao, “Graphene analogues of BN: Novel synthesis and properties,” *ACS Nano* **4**, 1539 (2010).
- Y. Kubota, K. Watanabe, O. Tsuda, and T. Taniguchi, “Deep ultraviolet light-emitting hexagonal boron nitride synthesized at atmospheric pressure,” *Science* **317**, 932 (2007).
- A. K. Sood, J. Menéndez, M. Cardona, and K. Ploog, “Resonance Raman scattering by confined LO and TO phonons in GaAs-AlAs superlattices,” *Phys. Rev. Lett.* **54**, 2111 (1985).
- P. C. Eklund, J. M. Holden, and R. A. Jishi, “Vibrational modes of carbon nanotubes; Spectroscopy and theory,” *Carbon* **33**, 959 (1995).
- D. González-García, D. Giordano, J. K. Russell, and D. B. Dingwell, “A Raman spectroscopic tool to estimate chemical composition of natural volcanic glasses,” *Chem. Geol.* **556**, 119819 (2020).
- X. Cong, X.-L. Liu, M.-L. Lin, and P.-H. Tan, “Application of Raman spectroscopy to probe fundamental properties of two-dimensional materials,” *npj 2D Mater. Appl.* **4**, 13 (2020).
- R. V. Gorbachev *et al.*, “Hunting for monolayer boron nitride: Optical and Raman signatures,” *Small* **7**, 465 (2011).
- M. Krečmarová, D. Andres-Penares, L. Fekete, P. Ashcheulov, A. Molina-Sánchez, R. Canet-Albiach, I. Gregora, V. Mortet, J. P. Martínez-Pastor, and J. F. Sánchez-Royo, “Optical contrast and Raman spectroscopy techniques applied to few-layer 2D hexagonal boron nitride,” *Nanomaterials* **9**, 1047 (2019).
- I. Stenger, L. Schué, M. Boukhicha, B. Berini, B. Plaçais, A. Loiseau, and J. Barjon, “Low frequency Raman spectroscopy of few-atomic-layer thick HBN crystals,” *2D Mater.* **4**, 31003 (2017).
- K. Zhang, Y. Feng, F. Wang, Z. Yang, and J. Wang, “Two dimensional hexagonal boron nitride (2D-HBN): Synthesis, properties and applications,” *J. Mater. Chem. C* **5**, 11992 (2017).
- T. M. G. Mohiuddin *et al.*, “Uniaxial strain in graphene by Raman spectroscopy: G peak splitting, Grüneisen parameters, and sample orientation,” *Phys. Rev. B* **79**, 205433 (2009).
- T. Azuhata, T. Sota, K. Suzuki, and S. Nakamura, “Polarized Raman spectra in GaN,” *J. Phys.: Condens. Matter* **7**, L129 (1995).
- T.-D. Huang, K. B. Simbulan, Y.-F. Chiang, Y.-W. Lan, and T.-H. Lu, “Symmetry breaking of in-plane Raman scattering by elliptically polarized light in MoS₂,” *Phys. Rev. B* **100**, 195414 (2019).
- S.-Y. Chen, C. Zheng, M. S. Fuhrer, and J. Yan, “Helicity-resolved Raman scattering of MoS₂, MoSe₂, WS₂, and WSe₂ atomic layers,” *Nano Lett* **15**, 2526 (2015).
- H. Oh, J. Jo, Y. Tchoe, H. Yoon, H. Hwi Lee, S.-S. Kim, M. Kim, B.-H. Sohn, and G.-C. Yi, “Centimeter-sized epitaxial h-BN films,” *NPG Asia Mater.* **8**, e330 (2016).

- ²⁰I. Calizo, W. Bao, F. Miao, J. Lau, and A. Balandin, "The effect of substrates on the Raman spectrum of graphene: Graphene on-sapphire and graphene-on-glass," *Appl. Phys. Lett.* **91**, 201904 (2007).
- ²¹N. Basu, M. S. Satya Bharathi, M. Sharma, K. Yadav, A. S. Parmar, V. R. Soma, and J. Lahiri, "Large area few-layer hexagonal boron nitride as a Raman enhancement material," *Nanomaterials* **11**, 622 (2021).
- ²²S. Hou, M. D. Birowosuto, S. Umar, M. A. Anicet, R. Y. Tay, P. Coquet, B. K. Tay, H. Wang, and E. H. T. Teo, "Localized emission from laser-irradiated defects in 2D hexagonal boron nitride," *2D Mater.* **5**, 15010 (2017).
- ²³P. Spizzirri, J. Fang, S. Rubanov, E. Gauja, and S. Praver, "Nano-Raman spectroscopy of silicon surfaces," *Mater. Forum* **34**, 161–166 (2010).
- ²⁴H. Fröhlich, "Interaction of electrons with lattice vibrations," *Proc. R. Soc. London, Ser. A* **215**, 291 (1952).